COMPARATIVE ANALYSIS ON SINGLE DIELECTRIC BARRIER DISCHARGE PLASMA ACTUATOR MODELS

Denis Palmeiro, Philippe Lavoie
Department of Aerospace Studies
University of Toronto
4925 Dufferin Street
Toronto, Ontario, Canada
M3H 5T6
denis.palmeiro@utoronto.ca;
lavoie@utias.utoronto.ca

ABSTRACT

Single-dielectric-barrier-discharge (SDBD) plasma actuators have shown much promise as an actuator for active flow control. Proper design and optimization of plasma actuators requires a model capable of accurately predicting the induced flow for a range of geometrical and excitation parameters. A number of models have been proposed in the literature, but have primarily been developed in isolation on independent geometries, frequencies and voltages. Many of these models rely on parameters that have been calibrated for one specific geometry. This study presents a comparison of four popular plasma actuator models over a range of actuation parameters for three different actuator geometries typical of actuators used in the literature. The results show that the hybrid model of Lemire & Vo (2011) is the only model capable of predicting the appropriate trends in how the body force and induced velocity change for different geometries. Additionally, it is the only model that exhibits a non-linear velocity scaling with voltage with a power law relationship of exponent 1.5, compared to the empirical result of a 3.5 power law found in the literature.

INTRODUCTION

Single-dielectric-barrier-discharge plasma actuators (herein denoted simply as plasma actuators) have become a popular type of actuator for many active flow control applications. Thus far, plasma actuators have most notably been applied in the areas of transition control (Grundmann & Tropea (2007); Hanson *et al.* (2010)), separation control by Corke *et al.* (2007), as well as noise control by Thomas *et al.* (2008) with much success. Design and optimization of plasma actuators depends on a model capable of accurately predicting the induced flow. While a number of models have been proposed throughout the literature, there has been no systematic study presenting the strengths and weaknesses of each model. More importantly, there has been no validation on the performance of these models for geometries other than the ones implemented in the studies used for their original calibration.

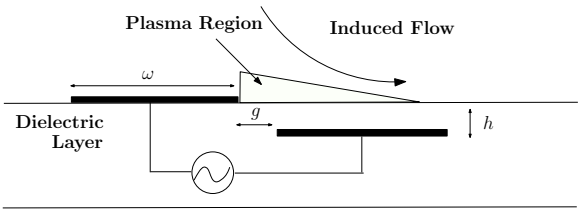

Figure 1. Plasma actuator geometrical configuration. ω, g, and h represent the electrode width, gap width spacing, and dielectric height, respectively.

Plasma actuators have a simple and robust design that consists of two electrodes separated by a dielectric, normally kapton or glass, in an asymmetric fashion as depicted in Figure 1. When a high voltage AC waveform of kHz frequency is applied to the exposed electrode, the assymetric geometry generates a plasma on the dielectric surface directly above the encapsulated electrode. The electrohydrodynamic coupling of the plasma and surrounding fluid generates an induced flow in the encapsulated electrode's direction. In a few hundred milliseconds, the induced flow forms into a steady wall jet, regardless of the time-dependent forcing that is involved. The induced wall jet is capable of reaching velocities up to 8 m/s in the wall-tangential direction (Moreau (2007)). Despite the large potential differences required to ignite the plasma, the power consumption of the plasma is in the range of 0.05-0.5 W/m (Pons *et al.* (2005)). This low power consumption coupled with the ability to deliver a real-time response in the kHz frequency to the surrounding fluid makes plasma actuators particularly attractive devices.

Generally, plasma actuators are designed following an ad hoc trial and error procedure. Given the many parameters that can be varied (electrode width, dielectric height, dielectric constant, applied waveform, driving frequency, applied voltage, gap width), it is difficult to predict the induced wall-jet, despite many parametric studies (e.g. Enloe *et al.* (2004*a*); Enloe *et al.* (2004*b*); Forte *et al.* (2007); Hoskinson

et al. (2008)). However, more recent efforts in model development has emerged to assist in the design process. For example, Likhanskii *et al.* (2007) reported that negative nanosecond pulses produce the most efficient performance when applied to their drift-diffusion type model. Additionally, Orlov & Corke (2006) developed a lumped-element circuit model, which they used to optimize for the maximum plasma extent across the dielectric surface.

Several parametric studies have been performed to determine the effect of various geometrical and excitation parameters on plasma actuator output. For example, Hoskinson *et al.* (2008) found an exponential increase in the thrust of the actuator as the thickness of the exposed electrode is decreased. Forte *et al.* (2007) also observed that an optimal gap width exists that maximizes the induced velocity. An important empirical trend of the plasma actuator, that has also been used by Orlov & Corke (2006) and Mertz & Corke (2009) as validation for their models, is the dependence on the applied voltage. Enloe *et al.* (2004*b*) measured an exponential relationship where $U_{max} \propto V^{7/2}$ was observed. A similiar result was also reported by Thomas *et al.* (2009), in which the thrust generated by the plasma actuator was measured and also confirmed to follow a 7/2 exponential relationship to voltage.

Previous work by Orlov & Corke (2006) has focused on the validation of plasma actuator models through comparisons with the plasma extent, and sweep out velocity. Furthermore, voltage scaling for power consumption was also measured and validated. Other authors primarily maintained their focus in reproducing the maximum velocity output observed through experiments. Mertz & Corke (2009) performed a comparison of the body force predicted for a selection of electric potential models. The present study takes the approach of Mertz & Corke (2009) a step further to investigate the performance of four popular plasma actuator models in predicting changes in both the generated body force and induced flow field due to variations in actuator geometry. Experimental measurements are used as part of this systematic comparison of these models. Furthermore, the scaling with respect to voltage of the body force and maximum induced velocity predicted by each model is compared and discussed with respect to published results.

PLASMA ACTUATOR MODELS

The most common way of modeling plasma actuators is to incorporate the Lorentz Force into the Navier-Stokes equations as a body force term. This decouples the plasma actuator from the Navier-Stokes and solutions for the applied force and resulting flow can be obtained independently. Plasma actuator models can be generally classified to belong to one of two families. The first consists of chemistry based models that attempt to spatially resolve the plasma phenomena directly. The second are algebraic models that are based on the solution of Poisson's equation. These algebraic models generally require assumptions regarding either the charge density or electric field produced by the actuator.

The chemistry based family typically consists of drift-diffusion type models such as Likhanskii *et al.* (2007), Singh & Roy (2007), and Jayaraman *et al.* (2008). These models track the chemical species present in the plasma, such as electrons and ions, using a set of transport equations. The essential plasma physics such as ionization, recombination, and streamer propogation are all modeled. In general, these models are capable of accurately resolving and predicting the plasma phenomena. However, the solution of these equations requires a very small spatial resolution on the order of μm to resolve the plasma phenomena. This imposes a significant restriction on the numerical time step and prohibits the calculation of high voltages at kilohertz frequencies. Because of this, the chemistry based family is not typically feasible for the design and optimization of plasma actuators.

For the above-mentioned reasons, the focus of the present study is on algebraic models, specifically the models proposed by Shyy *et al.* (2002), Suzen *et al.* (2005), Orlov & Corke (2006), Mertz & Corke (2009), and Lemire & Vo (2011). For convenience, they will be referred to as the SJA02, SH05, OC06, MC09, and LV11 models, respectively. Each one provides a unique method for calculating the generated Lorentz force by the plasma, alleviating the use of very fine spatial resolutions and time steps. A significant difference between these low-order algebraic models and the drift-diffusion type models is that the former generally involves assumptions on the behaviour of either the electric field or plasma charge density. We present below a brief description of the key aspects for the 4 models used in this work in the following paragraphs. More details about the models can be found in the original papers.

Shyy *et al.* (2002) suggested an algebraic model, approximating the electric field and assuming a spatially constant charge density. In this case, the electric field is assumed to decay linearly across the dielectric surface from a specified maximum value. The model is described by

$$E_o = \Delta V/g \Rightarrow |E| = E_o - k_1 x - k_2 y \tag{1}$$

$$E_x = \frac{Ek_1}{\sqrt{k_1^2+k_2^2}} \ , \ E_y = \frac{Ek_2}{\sqrt{k_1^2+k_2^2}} \tag{2}$$

$$\vec{F} = \nu \rho_c e_c \Delta t \delta \vec{E} \tag{3}$$

where k_1 and k_2 are constants representing the rate of electric field decay. The maximum electric field, E_o, is located at the trailing edge of the exposed electrode and is assumed to be equal to a parallel plate capacitor with the same potential difference as the plasma actuator.

In contrast, Suzen *et al.* (2005) solved the electric field by exploiting Gauss' Law. The two governing equations for the SH05 model are given by

$$\nabla \cdot (\varepsilon_r \nabla \phi) = 0 \tag{4}$$

$$\nabla \cdot (\varepsilon_r \nabla \rho_c) = \rho_c / \lambda_D^2 \tag{5}$$

Equation (5) represents Laplace's equation for an electrostatic potential and is solved using the applied voltage on the exposed electrode and grounded encapsulated electrode as boundary conditions. Poisson's equation for the spatial charge density, (6), was also implemented. The boundary condition for this case was a half-gaussian charge distribution on the dielectric surface, as described by

$$\rho_c^{BC} = \rho_c^{max} \exp[-(x-\mu)/(2\sigma^2)] \tag{6}$$

where ρ_c^{max}, μ, and σ represent the maximum charge density, position of the exposed electrode trailing edge, and the half-gaussian shape factor, respectively. The values for ρ_c^{max} and λ_D were arbitrarily defined by Suzen *et al.* (2005) as $8 \cdot 10^{-4}$ C/m^3, and 0.001 m to match the flow results of Jacob *et al.* (2005).

Orlov & Corke (2006) proposed a more complex model by implementing the existence of a series of virtual electrodes on the dielectric surface. Formulating the actuator as an electric circuit provides a set of governing ODEs for the virtual electrode series, viz.

$$\frac{dV_n(t)}{dt} = \frac{dV_{app}(t)}{dt}\left(\frac{C_{an}}{C_{an}+C_{dn}}\right) + k_n \frac{I_{pn}(t)}{C_{an}+C_{dn}} \quad (7)$$

The solution provides the voltage on the virtual electrode that is further applied as a third boundary condition for the electric potential. As shown by Mertz (2010), however, the OC06 model incorrectly predicts the direction of induced flow. An updated version was suggested by Mertz & Corke (2009) by reversing the sign of the potential on the virtual electrode. While this modification continues to produce a significant flow in the upstream direction, a downstream directed flow is also generated. This upstream flow behaviour is not present in the PIV results of Post (2004) and Balcon *et al.* (2009), and appears to be an artifact generated by the MC09 and OC06 models.

The Lorentz force of the MC09 and OC06 models is solved in a similiar approach to the SH05 model using a slightly altered form of Poisson's equation,

$$\nabla \cdot (\varepsilon_r \nabla \phi) = \phi / \lambda_D^2 \quad (8)$$

$$\vec{f}_B = \left(\frac{\varepsilon_o}{\lambda_D^2}\right)\phi \nabla \phi \quad (9)$$

For these models, parameters that cannot be measured such as the plasma height, and plasma resistivity are defined to match the experimentally measured extent, and sweep out velocities of the plasma. As presented, however, the MC09 model generated velocity magnitudes of up to 30 m/s in the present simulations. Since such high velocities were not measured experimentally either in this study or elsewhere in the literature,, the magnitude of the force field was reduced by a factor of 0.25 in this study to produce more comparitive velocity magnitudes.

Finally, Lemire & Vo (2011) combined the SH05 and OC06 models into a single hybrid model. The virtual electrode concept is further extended into the LV11 model, and the definitions of the plasma height, and resistivity parameters are also retained. Calculation of the charge density, electric potential, and Lorentz force all follow directly from the SH05 model through (5)-(6), however in this case the half-gaussian boundary condition is replaced with the following function that is obtained through (8),

$$\rho^{BC} = \frac{I_{pn} \cdot \Delta t}{Volume_n} \quad (10)$$

where I_{pn}, Δt, and $Volume_n$, represent the plasma current through the n^{th} virtual electrode, the computational time step, and volume of plasma at the n^{th} virtual electrode, respectively.

A common feature amongst each of the above models is the need for empirical calibration. For example, the SJA02 model defines a charge density that is spatially constant and acts as a scaling parameter to the electric field. The SH05 model has a similiar dependence on the maximum charge density and debye length parameters which are specified to match the simulated flow with experiments. The OC06, MC09, and LV11 models all share the same empirical parameters in the form of plasma height, and resistivity. In these cases, the values have been prescribed to match the plasma extent and sweep out velocities measured by Enloe *et al.* (2004*b*) using a photomultiplier tube. Since the parameters of each model has been specified based on experimental results obtained on one actuator geometry only, it is not clear how general these are as the actuator geometry is changed.

EXPERIMENTAL AND NUMERICAL DETAILS

Four different comparisons are made to test the performance of each model across different geometries. Each model is tested on three geometries and voltages that are representative of the range of actuators used in the literature. Empirical parameters remain unchanged from the original specifications given in the original paper introducing the method. The configuration of each actuator for this comparison is specified in Table 1.

Table 1. Plasma Actuator Configurations

Geometry	A	B	C
Electrode Width (mm)	6.35	12.7	5
Electrode Gap (mm)	1	1	0
Dielectric Height (mm)	0.19	0.57	0.18
Dielectric Constant	2.9	2.9	2.9
Applied Voltage (kVpp)	12	15	10
Frequency (kHz)	3	3	2.75
Downstream Location (mm)	6	10	10

Vertical velocity profiles were measured using a 0.45 mm diameter glass pitot tube in quiescent air. The probe was directed to measure the streamwise velocity and mounted to a vertical traverse with a resolution of 3 μm. Results were measured using a pressure transducer capable of measuring up to 1 mbar. The downstream location of the measurement for each actuator is specified in Table 1. Each excitation signal was sinusoidal and was delivered using a Rigol DG1011 waveform generator amplified by a Trek 20/20C High Voltage Amplifier.

The body force distribution computed with each model was introduced in a Navier-Stokes solver to compute the resulting velocity field induced by the plasma actuators. The OpenFOAM CFD software suite was implemented using a second order backwards-biased time marching scheme and second order central spatial differencing. The time step was defined to maintain a Courant number below 0.1, and simulations were completed when the wall-jet formed by the actuator reached a steady-state, typically after 300 ms. The CFD domain size was constrained to 10 cm in the y-direction, and 60

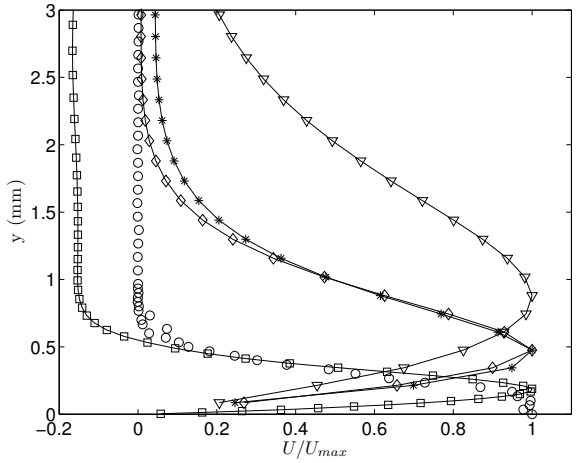

(a) Vertical Velocity Profiles on Geometry A

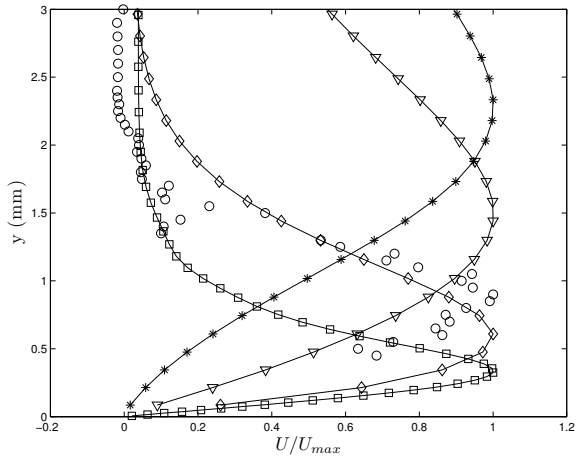

(b) Vertical Velocity Profiles on Geometry B

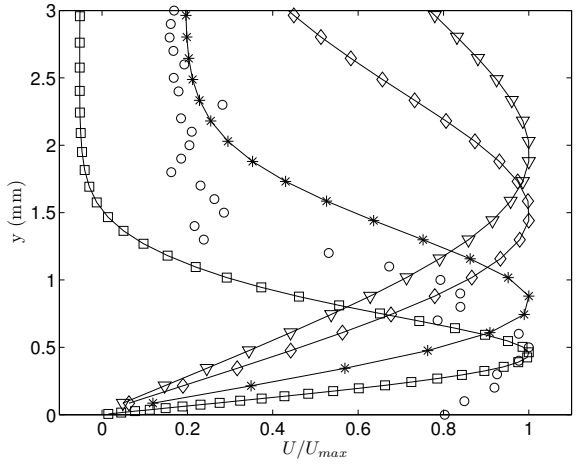

(c) Vertical Velocity Profiles on Geometry C

Figure 2. Experimental vertical velocity profiles compared against simulations over three geometries. Legend: ◯ Experiment -♢- SJA02 -□- MC09 -▽- SH05 -∗- LV11

cm in the x-direction. The body force of the plasma actuator is applied at the 10 cm position from the left boundary, allowing 50 cm in the downstream location for the induced flow. The no slip boundary condition was applied to the dielectric surface and a zero gradient velocity to the top and side boundaries of the domain. The pressure was fixed to be zero on the top and side boundaries, and a zero gradient condition was also applied to the dielectric surface. A stretched grid was implemented in the domain to resolve the location of the body force. The minimum cell size was $3\mu m$ in the y-direction, and $15.5\mu m$ in the x-direction for the MC06 model, and $43\mu m$ in the y-direction and 156 μm in the x-direction for all other models. A total of 120,000 cells was also used in the CFD simulations.

RESULTS

Figure 1 shows the vertical profiles of streamwise velocity obtained from each model as well as experiments. In order to facilitate comparison, each profile is normalised by its maximum velocity, which is listed in Table 2. From these results, it is clear that there are significant differences between the flow field predicted by each model. Furthermore, none of the models are able to reproduce the experimental data. It is important to note the shape of the induced wall-jet profile. The shape is strongly affected by the magnitude of the body force. For a given force distribution, as the magnitude is increased, the profile shape becomes more narrow and the maximum velocity increases. Therefore, in cases in which the maximum velocities are nearly comparable or higher than the experiments, the width of the profiles compare much more closely with the empirically measured ones.

Table 2. Maximum Velocities on Each Configuration

	A	B	C
Experiment (m/s)	1.9458	1.2772	1.5181
SJA02 (m/s)	0.7266	0.8383	0.3042
SH05 (m/s)	0.2110	0.2495	0.2124
MC09 (m/s)	8.9311	7.3674	3.9770
LV11 (m/s)	1.5339	0.2927	1.2382

The results for the SJA02 model show an underprediction of the flow. This model depends strongly on the maximum electric field, defined by $E = \Delta V/g$, where ΔV and g are the potential difference and gap width, respectively. Since there is no dependence on the dielectric height, the SJA02 model relies solely on the applied voltage to calculate the body force. This is also reflected in the results of Table 2 where the model is unable to capture the decreasing velocity trend from geometry A to B. The decreasing velocity is caused by the dramatic increase in dielectric height, yet the SJA02 model is focused on the increase in applied voltage.

Results from the SH05 model also demonstrates a lack of generality with respect to geometry. This is due to the arbitrarily defined charge density boundary condition that remains fixed for all configurations. Since this model is very sensitive

to the spatial charge density, an accurate representation of this distribution is critical for the model to yield accurate predictions.

The LV11 model provides a correction to the fixed charge density limitation of the SH05 model. Using the charge density distribution predicted through the electric circuit model defined by Orlov & Corke (2006), it is capable of accounting for changes in geometry, voltage, and frequency. The LV11 model also underpredicts the maximum velocity, however, it is significantly closer to that measured in the experiments.

It is important to take note of the underlying trends that exist between the different geometries. For example, despite having applied the largest voltage, geometry B produced the smallest velocity in the experiments. Further, a decrease in velocity is also experienced from geometry A to C. These trends are critical as they provide a test on whether the model can accurately capture these changes. The only model that is capable of capturing these geometrical trends is the LV11 model. It correctly predicts a decrease in velocity from A to C, and the lowest velocity is also exhibited by B despite the underprediction to the measured values. As expected, the SJA02 model predicts a maximum velocity on geometry B where the largest potential difference is applied. The SH05 model also predicts the highest velocity on geometry B, while the results on the other geometries are approximately equal. This could be a result of the maximum charge density implemented in the surface boundary condition. Since it is a constant value across all actuators, it is unable to adjust to any changes in geometry or electric field intensity. The MC09 model is able to capture the geometrical changes from A to B, however, the lowest velocity is generated from geometry C. Clearly, the implementation of the diffusion equation for the charge density appears to make a significant contribution when combined with the electric circuit treatment of the OC06 and MC09 models, as implemented in the LV11 model.

An important property of plasma actuators is the induced body force dependence on the applied voltage. Figure 3a shows a plot of the induced body force as a function of applied voltage. In this case, 1.27 cm wide electrodes with zero gap width were separated by a 0.2 mm thick glass sheet with a dielectric constant of 6.1. The maximum force is calculated by the time RMS of the spatially averaged force field, as previously performed in Mertz & Corke (2009). The MC09 and LV11 models are the only models that represent a non-linear behaviour reflected by the power law relationship with exponents of 3.7 and 4.0, respectively. A similiar relationship was reported by Mertz & Corke (2009) for the MC09 model.

The voltage scaling for the maximum velocity is also evaluated to provide a further comparison and is shown in Figure 3b. In order to prove a comparable scale on which to evaluate the underlying trends, each model was normalised by the maximum velocity obtained at a voltage of 20 kV_{pp}. From the figure, the variation in the predicted velocity for MC09 and LV11 with voltage show a significant deviation from the power-law observed for the induced body force. In the case of MC09, the velocity produced by the plasma actuator follows approximately a linear relationship. This appears to be a consequence of the actual direction of the body force vector calculated by each model (not only the force magnitude). From Figure 3b, the only model that demonstrates a slightly non-linear behaviour is the LV11 model with a power law relationship of exponent 1.5. This behaviour is most closely related to the experimental results obtained by Enloe *et al.* (2004*b*) where a $7/2$ power law relationship was observed, although there is still a large difference in the two exponential relationships.

CONCLUSION

A comparison of four popular plasma actuator models was presented over three different actuator configurations. Each configuration involved a variation in geometry and voltage to evaluate the generality of each model. The only model to capture the proper direction of changes in the induced velocity between each geometry was the LV11 model proposed by Lemire and Vo (2011). Furthermore, it was also the only model able to predict velocity magnitudes that were comparable to the experiments on two out of the three configurations. The SJA02 and SH05 models generally underpredicted the velocities in every case, while the MC09 model drastically overpredicted the induced velocity. The underlying issue for these results is the existence of model parameters that have been predefined on specific actuator geometries for a specific excitation voltage and frequency. This has very important implications when considering the use of these models for the purpose of designing the optimal actuator geometry for a particular application since the models would require recalibration for each actuator configuration to be considered.

Furthermore, the predictions of each model as a function of voltage for a given geometry were compared. Results were shown for both velocity, and body force magnitude. The only model that exhibited a slightly non-linear relationship for the maximum velocity with voltage is the LV11 model. While this relationship was still significantly different than the reported behaviour from the literature, it was still the only model capable of producing a non-linear trend. The remaining models all demonstrated linear trends for the velocity contrary to empirical observations.

Finally, it appears that the hybrid approach by Lemire & Vo (2011) represents the most accurate plasma actuator behaviour from the models evaluated in this study. Although the model has difficulty dealing with thick dielectrics, it provides an approach that can potentially be used for actuator design optimization. A modification for the experimental parameters that are present within the LV11 model may provide a suitable correction when extrapolating to alternate geometries.

ACKNOWLEDGEMENTS

This work was supported and funded by the Natural Sciences and Engineering Research Council of Canada. The authors would like to thank B. E. Mertz and T. C. Corke for helpful discussions regarding the OC06 and MC09 models.

REFERENCES

Balcon, N., Benard, N. & Moreau, E. 2009 Formation process of the electric wind produced by a plasma actuator. *IEEE Transactions on Dielectrics and Electrical Insulation* **16**, 463–469.

Corke, T., Post, M. & Orlov, D. 2007 SDBD plasma enhanced aerodynamics: concepts, optimization and applications. *Progress in Aerospace Sciences.* **43**, 192–217.

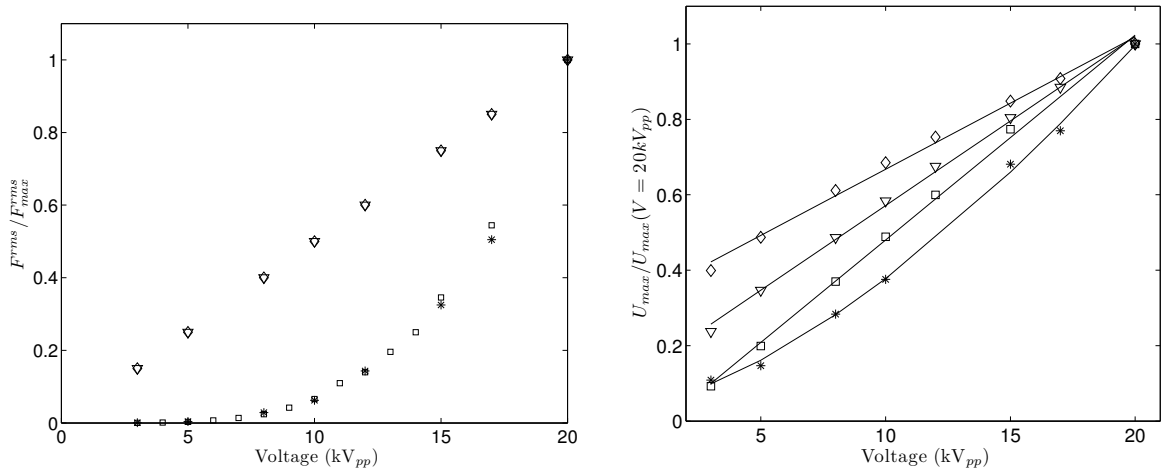

(a) Time-rms, spatially averaged force as a function of voltage (b) Normalised maximum velocity as a function of the voltage

Figure 3. Empirical trends for the time-rms spatially averaged force and maximum velocity as a function of voltage. Legend: -$\diamondsuit$- SJA2002 -$\square$- MC2009 -$\triangledown$- SH2005 -$*$- LV2011

Enloe, C. L., McLaughlin, T. E., VanDyken, R. D., Kachner, K.D., Jumper, E. J. & Corke, T. C. 2004*a* Mechanisms and responses of a single dielectric barrier plasma actuator: Plasma morphology. *AIAA J.* **42** (3), 589–594.

Enloe, C. L., McLaughlin, T. E., VanDyken, R. D., Kachner, K.D., Jumper, E. J., Corke, T. C., Post, M. & Haddad, O. 2004*b* Mechanisms and responses of a single dielectric barrier plasma actuator: Geometric effects. *AIAA J.* **42** (3), 595–604.

Forte, M., Jolibois, J., Pons, J., Moreau, E., Touchard, G. & Cazalens, M. 2007 Optimization of a dielectric barrier discharge actuator by stationary and non-stationary measurements of the induced flow velocity: application to airflow control. *Exp. Fluids.* **43**, 917–928.

Grundmann, S. & Tropea, C. 2007 Experimental transition delay using glow-discharge plasma actuators. *Exp. Fluids.* **42** (4), 653–657.

Hanson, R. E., Lavoie, P., Naguib, A. M. & Morrison, J. F. 2010 Transient growth instability cancelation by a plasma actuator array. *Exp. Fluids.* pp. 1–10.

Hoskinson, A. R., Hershkowitz, N. & Ashpis, D. E. 2008 Force measurements of single and double barrier DBD plasma actuators in quiescent air. *J. Appl. Phys.* **41**, 1–9.

Jacob, J.D., Ramakumar, K., Anthony, R. & Rivir, R.B. 2005 Control of laminar and turbulent shear flows using plasma actuators. *4th International Symposium on Turbulence and Shear Flow Phenomena* .

Jayaraman, B., Cho, Y. & Shyy, W. 2008 Modeling of dielectric barrier discharge plasma actuator. *J. Appl. Phys.* **103** (5), 053304.

Lemire, S. & Vo, H. D. 2011 Reduction of fan and compressor wake defect using plasma actuation for tonal noise reduction. *Journal of Turbomachinery.* **133**.

Likhanskii, A., Shneider, M., Macheret, S. & Miles, R. 2007 Modeling of dielectric barrier discharge plasma actuators driven by repetitive nanosecond pulses. *Physics of Plasmas.* **14**.

Mertz, B. & Corke, T. 2009 Time-dependent dielectric barrier discharge plasma actuator modeling. *47th AIAA Aerospace Sciences Meeting Including The New Horizons Forum and Aerospace Exposition in Orlando Florida.* **2009-1083**.

Mertz, B. E. 2010 Refinement, validation, and implementation of lumped circuit element model for single dielectric barrier discharge plasma actuators. PhD thesis, University of Notre Dame.

Moreau, E. 2007 Airflow control by non-thermal plasma actuators. *J. Appl. Phys.* **40**, 605–636.

Orlov, D. M. & Corke, T. C. 2006 Electric circuit model for aerodynamic plasma actuator. *44th AIAA Aerospace Sciences Meeting and Exhibit in Reno, Nevada.* **2006-1206**.

Pons, J., Moreau, E. & Touchard, G. 2005 Asymmetric surface dielectric barrier discharge in air at atmospheric pressure: electric properties and induced airflow characterists. *J. Appl. Phys.* .

Post, M. L. 2004 Plasma actuators for separation control on stationary and unstationary airfoils. PhD thesis, University of Notre Dame.

Shyy, W., Jayaraman, B. & Andersson, A. 2002 Modeling of glow discharge-induced fluid dynamics. *J. Appl. Phys* **92** (11), 6434–6443.

Singh, K. & Roy, S. 2007 Modeling plasma actuators with air chemistry for effective flow control. *J. Appl. Phys* **101**.

Suzen, Y. B., Huang, P. G. & Jacob, J. D. 2005 Numerical simulations of plasma based flow control applications. *35th AIAA Fluid Dynamics Conference and Exhibit in Toronto, Ontario.* **2005-4633**.

Thomas, F, and Corke T, Iqbal, M, Kozlov, A & Schatzman, D 2009 Optimization of dielectric barrier discharge plasma actuators for active aerodynamic flow control. *AIAA J.* **47**, 2169–2178.

Thomas, F, Kozlov, A & T, Corke. 2008 Plasma actuators for cylinder flow control and noise reduction. *AIAA J.* **46**, 1921–1931.